Electronic Supplementary Information (ESI)

Ni-doping Optimized d-Band Center in Bifunctional Fe_2O_3 Modified by Bamboo-Like NCNTs as Cathode Material for Zn-air Battery

Yang Shi [a], Songhan Hu [b], Xinxin Xu [a] * and Jin Chen [b]

[a] Department of Chemistry, College of Science, Northeastern University, Shenyang 110819, Liaoning, China

[b] Key Laboratory of Electromagnetic Processing of Materials, MOE, Northeastern University, Shenyang 110819, Liaoning, China

Materials and characterization

All chemicals were of analytical grade, commercially available from Sinopharm Chemical Reagent Co. Ltd and used as received without further purification. PXRD pattern was recorded on X-ray diffractometer with CuK_α (λ = 1.5418 Å) radiation (Philips X'Pert Pro Super, Philips). Raman spectroscopy was conducted with an excitation wavelength of 633 nm (LabRAMHR-800, Horiba). XPS and UPS were performed on photoelectron spectroscopy (ESCALAB 250Xi, Thermo Fisher Scientific). The morphology was observed on an ultra plus field emission scanning electron microscope (SEM, ultra plus, ZEISS) and transmission electron microscopy (TEM, JEOL, JEM-2100F). Electrochemical tests were conducted on electrochemical workstation (CHI-760E, Chenhua).

RRDE test in ORR

RRDE (electrode area is 0.2475 cm^2) experiment was also conducted in O_2 saturated KOH (0.1 M). Working electrode was fabricated as follows: the mixture of **Ni/Fe-Fe_2O_3@NCNTs** (or **Fe-Fe_2O_3@NCNTs**, 2 mg) and carbon black (Vulcan XC-72R, 8 mg) was dispersed in aqueous solution of water (0.8 mL), ethanol (0.15 mL) and 50 μL Nafion (5 %). The ink (10 μL) was dropped on RRDE and served as working electrode. Pt wire and Ag/AgCl electrode (3 M KCl) were employed as counter and reference electrodes. The disk potential was cycled from 0 to 1.0 V (vs. RHE) with a scan rate of 10 $mV \cdot s^{-1}$. The ring potential was constant at 1.2 V (vs. RHE). The H_2O_2 selectivity and electron transfer number (n) were calculated with Eq. 1 and 2. In these equations, I_D and I_R represent the disk and ring currents density. N (N = 0.37, obtained from $K_3Fe(CN)_6$ reduction experiments at various rotation rates) is the current collection efficiency of the Pt ring. To study ORR activity with RRDE method,

PBS (0.1 M, pH=7.4) saturated by O_2 was employed as electrolyte.

$$H_2O_2\ \% = (200 \times I_R/N)/(I_R/N + I_D)\ (1)$$

$$n = 4 \times I_d/(I_R/N + I_D)\ (2)$$

RDE test in ORR

RDE test was conducted in O_2 saturated KOH (0.1 M) with three-electrode system, in which Pt wire and Ag/AgCl electrode (3 M KCl) were employed as counter and reference electrodes. Working electrode was fabricated as follows: the mixture of **Ni/Fe-Fe_2O_3@NCNTs** (or **Fe-Fe_2O_3@NCNTs**, 2 mg) and carbon black (Vulcan XC-72R, 8 mg) was dispersed in aqueous solution of water (0.8 mL), ethanol (0.15 mL) and 50 μL Nafion (5 %). The ink (10 μL) was dropped on RDE (electrode area is 0.196 cm^2) and served as working electrode. Linear sweep voltammetry (LSV) was recorded at 10 $mV \cdot s^{-1}$. The rotating speed of RDE was 400, 625, 900, 1225, 1600, 2025 and 2500 rpm. The electron transfer number was calculated by using the Koutechy-Levich (K-L) equation (Eq. 3). In this equation, j is the measured current density, j_k is the kinetic current density, ω is the electrode rotating rate. The parameter B could be calculated from the slope of the K-L plots based on the following Levich equation (Eq. 4), in which n is the electron transfer number per oxygen molecule, F is the Faraday constant (F = 96485 $C \cdot mol^{-1}$), D_0 is the diffusion coefficient of O_2 in 0.1 M KOH (D_0 = 1.9×10^{-5} $cm^2 \cdot s^{-1}$), *v* is the kinetic viscosity (*v* = 0.01 $cm^2 \cdot s^{-1}$) and C_0 is the bulk concentration of O_2 (C_0 = 1.2×10^{-6} $mol \cdot cm^{-3}$). To study ORR activity with RDE method, PBS (0.1 M, pH=7.4) saturated by O_2 was employed as electrolyte.

$$1/j = 1/j_k + 1/B\omega^{1/2}\ (3)$$

$$B = 0.62nF(D_0)^{2/3}(V)^{-1/6}C_0\ (4)$$

OER test

OER was conducted in N_2 saturated KOH (1 M). Three-electrode system was employed. Working electrode was fabricated as follows: the mixture of **Ni/Fe-Fe_2O_3@NCNTs** (or **Fe-Fe_2O_3@NCNTs**, 2 mg) and carbon black (Vulcan XC-72R, 8 mg) was dispersed in aqueous solution of water (0.8 mL), ethanol (0.15 mL) and 50 μL Nafion (5 %). The ink (10 μL) was dropped on glassy carbon (GC) electrode (electrode area is 0.196 cm^2). In this system, Pt wire and Ag/AgCl electrode (3 M KCl) were employed as reference electrode and counter electrode, respectively. LSV curves were recorded at 5 $mV \cdot s^{-1}$.

Zn-air battery assemble

Zn-air battery was assembled with a home-made cell in the size of 4.2 × 4 × 4 cm^3. The Zn plate with working area 3.2 cm^2 acts as anode. **Ni/Fe-Fe_2O_3@NCNTs** ink (fabricated as mentioned ORR and OER tests) was casted on carbon paper equipped with air diffusion layer, which was employed as air cathode. The working area of air cathode is also 3.2 cm^2. The cell was filled with 25 mL mixed solution of KOH (6.0 M) and $Zn(OAc)_2$ (0.2 M). No additional O_2 was inlet into this battery. To assemble Zn-air battery with neutral electrolyte, the mixed solution of NH_4Cl (4 M) and KCl (1 M) was employed as selected.

Theoretical calculation details

Density functional theory (DFT) calculations about the ORR/OER were performed using the Vienna ab initio simulation package (VASP). The projector augmented wave (PAW) method was employed. The generalized gradient approximation (GGA) of Perdew-Burke-Ernzerhof (PBE) was used to estimate electron-electron exchange and correlation functional. In our calculation, we used plane-wave basis set with 400 eV kinetic energy cutoff and the Brillouin zone was sampled by the Monkhorst-Pack

method with 3×3×1 k-point grids. Gibbs free energy change of each elementary step was calculated with the following equation (Eq. 5). In this equation, T is 298.15 K, E is the reaction energy calculated by the DFT method, ZPE and ΔS are the changes in zero-point energies and entropy in the reaction. For ΔG_U = -neU, it represents the applied potential (U) effect on reaction concerning electron (e) in the electrode and n is electron transfer number of elementary reaction.

$$\Delta G = \Delta E + \Delta ZPE - T \cdot \Delta S + \Delta G_U \quad (5)$$

The over-potential of ORR/OER can be determined by computing Gibbs free energies of the reaction at different elementary steps. Thermo-chemistry parameters of the reactions were obtained by DFT computations along with the computational hydrogen electrode (CHE) model. The ORR and OER could be described Table S3.

Table S1. Comparison ORR activity of **Ni/Fe-Fe_2O_3@NCNTs** with other materials

Catalyst	**$E_{1/2}$**	**Limiting current density**	**n value**	**Ref.**
Fe/Co-N/$S_{1.9}$-C	0.836 V	5.44 mA cm^{-2}	3.95	S1
$CoFe_2O_4$-N,S-C	0.840 V	5.25 mA cm^{-2}	3.90	S2
$CoFe_2O_4$/CNTs/FA-500	0.808 V	5.40 mA cm^{-2}	3.96	S3
Co-SAs/N-C/rGO	0.840 V	4.51 mA cm^{-2}	3.94	S4
G-CoNOC	0.880 V	3.0 mA cm^{-2}	~4	S5
Ni/Fe-Fe_2O_3@NCNTs	**0.946 V**	**5.35 mA cm^{-2}**	**3.92-4.04**	**Here**

Table S2. Comparison OER activity of **Ni/Fe-Fe_2O_3@NCNTs** with other materials

Catalyst	**Overpotential (η_{10})**	**Tafel**	**Ref.**
$CoFe/NC_{30\%}$	340 mV	77.0 mV dec^{-1}	S6
CFO@CSs	390 mV	57.7 mV dec^{-1}	S7
$CuFe_2O_4$	369 mV	76.3 mV dec^{-1}	S8
$FeCo@CoN_x@FeP_x/C$	368 mV	70.1 mV dec^{-1}	S9
Fe/12Zn/Co-NCNTs	343 mV	92.5 mV dec^{-1}	S10
Ni/Fe-Fe_2O_3@NCNTs	**388 mV**	**89.1 mV dec^{-1}**	**Here**

Table S3. The reaction routes in ORR and OER

	In ORR	**In OER**
1	$O_2 + H_2O + e = OOH^* + OH^-$	$OH^- - e = OH^*$
2	$OOH^* + e = O^* + OH^-$	$OH^* + OH^- - e = O^* + H_2O$
3	$O^* + H_2O + e = OH^* + OH^-$	$O^* + OH^- - e = OOH^*$
4	$OH^* + e = OH^-$	$OOH^* + OH^- - e = O_2 + H_2O$

Table S4. Comparison the ZAB performance of **Ni/Fe-Fe_2O_3@NCNTs** with recently reported materials.

Catalyst	**Power density**	**Specific capacities (10 mA cm^{-2})**	**Ref.**
Co-NCNTFs	158 mW cm^{-2}	795 mAh g^{-1}	S11
Fe/Cu-N-C	183 mW cm^{-2}	805 mAh g^{-1}	S12
P-FeCo/NC	115 mW cm^{-2}	760.39 mAh g^{-1}	S13
Co_{SA}-RuO_2-NUCN	156.6 mW cm^{-2}	766.14 mAh g^{-1}	S14
F NH_2-FeNi-800	123.8 mW cm^{-2}	813.3 mAh g^{-1}	S15
Ni/Fe-Fe_2O_3@NCNTs	**170.1 mW cm^{-2}**	**819.8** mAh g^{-1}	**Here**

References

(S1) Cai, J.; Xu, Y.; Sun, Y.; Zhao, H.; Ye, D.; Tang, Y.; Sun, C.; Liu, L.; Zhang, J. Regulating the coordination environment of Fe/Co-N/S-C to enhance ORR and OER bifunctional performance. *Inorg. Chem. Front.* **2023,** *10*, 1826-1837.

(S2) Xiao, Z.; Lv, X.; Liu, S.; Liu, Q.; Wang, F.; Yan, W.; Xing, T.; Li, Z.; Li, X.; Chen, Y. Electronic Band Structure Engineering of Transition Metal Oxide-N,S-Doped Carbon Catalysts for Photoassisted Oxygen Reduction and Oxygen Evolution Catalysis. *Adv. Mater. Interfaces* **2021,** *9,* 2101386.

(S3) Huang, Q.; Li, C.; Tu, Y.; Jiang, Y.; Mei, P.; Yan, X. Spinel $CoFe_2O_4$/carbon nanotube composites as efficient bifunctional electrocatalysts for oxygen reduction and oxygen evolution reaction. *Ceram. Int.* **2021,** *47*, 1602-1608.

(S4) Li, L.; Li, N.; Xia, J.; Zhou, S.; Qian, X.; Yin, F.; He, G.; Chen, H. Metal-organic framework-derived Co single atoms anchored on N-doped hierarchically porous carbon as a pH-universal ORR electrocatalyst for Zn-air batteries. *J. Mater. Chem. A* **2023,** *11*, 2291-2301.

(S5) Geng, D.; Huang, Y.; Yuan, S.; Jiang, Y.; Ren, H.; Zhang, S.; Liu, Z.; Feng, J.; Wei, T.; Fan, Z. Coordination Engineering of Defective Cobalt-Nitrogen-Carbon Electrocatalysts with Graphene Quantum Dots for Boosting Oxygen Reduction Reaction. *Small* **2023**, *19*, No. e2207227.

(S6) Gebreslase, G. A.; Martinez-Huerta, M. V.; Sebastian, D.; Lazaro, M. J. Transformation of $CoFe_2O_4$ spinel structure into active and robust CoFe alloy/N-doped carbon electrocatalyst for oxygen evolution reaction. *J. Colloid Interface Sci.* **2022,** *625*, 70-82.

(S7) Alhakemy, A. Z.; Elseman, A. M.; Fayed, M. G.; Ahmed Amine Nassr, A. B.; El-Hady Kashyout, A.; Wen, Z. Hybrid electrocatalyst of $CoFe_2O_4$ decorating carbon spheres for alkaline oxygen evolution reaction. *Ceram. Int.* **2022,** *48*, 5442-5449.

(S8) Ferreira, L. S.; Silva, T. R.; Silva, V. D.; Raimundo, R. A.; Simões, T. A.; Loureiro, F. J. A.; Fagg, D. P.; Morales, M. A.; Macedo, D. A. Spinel ferrite MFe_2O_4 (M = Ni, Co, or Cu) nanoparticles prepared by a proteic sol-gel route for oxygen evolution reaction. *Adv. Powder Technol.* **2022,** *33,* 103391.

(S9) Ding, W.; Saad, A.; Wu, Y.; Wang, Z.; Li, X. CNTs/CNF-supported multi-active components as highly efficient bifunctional oxygen electrocatalysts and their applications in zinc-air batteries. *Nano Res.* **2023**.

(S10) Xue, J.; Deng, S.; Wang, R.; Li, Y. Efficient synergistic effect of trimetallic organic frameworks derived as bifunctional catalysis for the rechargeable zinc-air flow battery. *Carbon* **2023,** *205*, 422-434.

(S11) Sun, Z.; Ding, Y.; Wang, C.; Mao, P.; Wang, B.; Ran, R.; Zhou, W.; Liao, K.; Shao, Z. A magnetic binder-linked air electrode with anti-pulverization behavior for rechargeable and recyclable Zn-air batteries. *Adv. Funct. Mater.* **2023,** *33*, 2302234.

(S12) Bu, M.; Liu, Y.; Liao, S.; Liu, W.; Yang, Z.; Jiang, J.; Gao, X.; Yang, Y.; Liu, H. In-site grown carbon nanotubes connecting Fe/Cu-N-C polyhedrons as robust electrocatalysts for Zn-air batteries. *Carbon* **2023,** *214*, 118365.

(S13) Wang, N.; Mei, R.; Chen, L.; Yang, T.; Chen, Z.; Lin, X.; Liu, Q. P-bridging asymmetry diatomic catalysts sites drive efficient bifunctional oxygen electrocatalysis for zinc-air batteries. *Small* **2024,** e2400327.

(S14) Ma, X.; Liu, M.; Li, Q.; Xiao, X.; Liu, J.; Xu, X.; Yin, Y.; Qiao, P.; Zhang, L.; Zou, X.; et al. Associating Co single atoms with RuO_2 nanoparticles anchor on nitrogen-doped

ultrathin porous carbon nanosheets as effective bifunctional oxygen electrocatalysts for rechargeable Zn-air batteries. *J. Mater. Chem. A* **2023,** *11*, 16889-16899.

(S15) Wang, X.; Li, K.; Yang, D.; Yang, X.; Xiao, M.; Zheng, L.; Xing, W.; Liu, C.; Zhu, J. F doping-induced multicomponent synergistic active site construction toward high-efficiency bifunctional oxygen electrocatalysis for rechargeable Zn-air batteries. *Small* **2024,** *20*, e2310250.

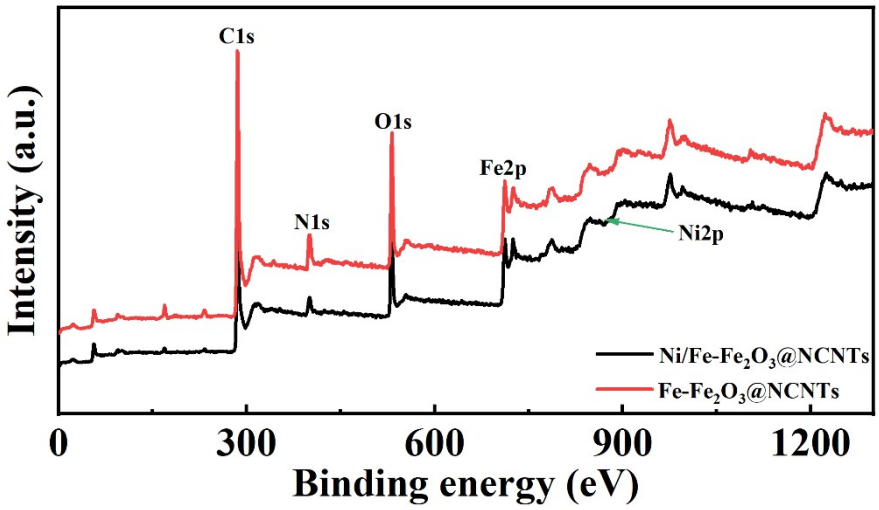

Fig. S1. XPS survey spectra of **Ni/Fe-Fe_2O_3@NCNTs** and **Fe-Fe_2O_3@NCNTs**.

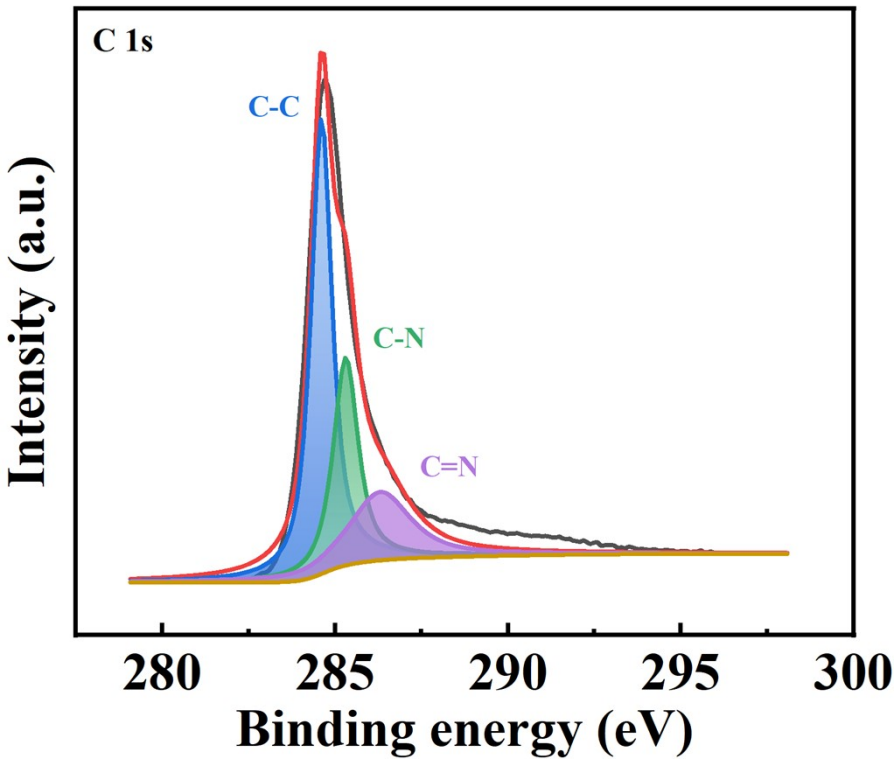

Fig. S2. XPS high resolution C 1s spectrum of **Ni/Fe-Fe_2O_3@NCNTs**.

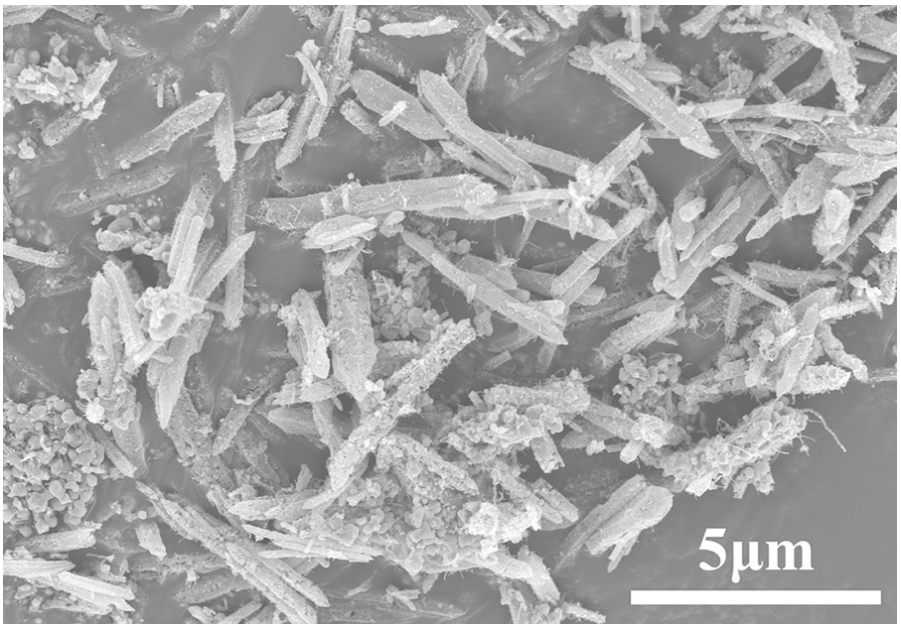

Fig. S3. SEM image of **Ni/Fe-Fe_2O_3@NCNTs**.

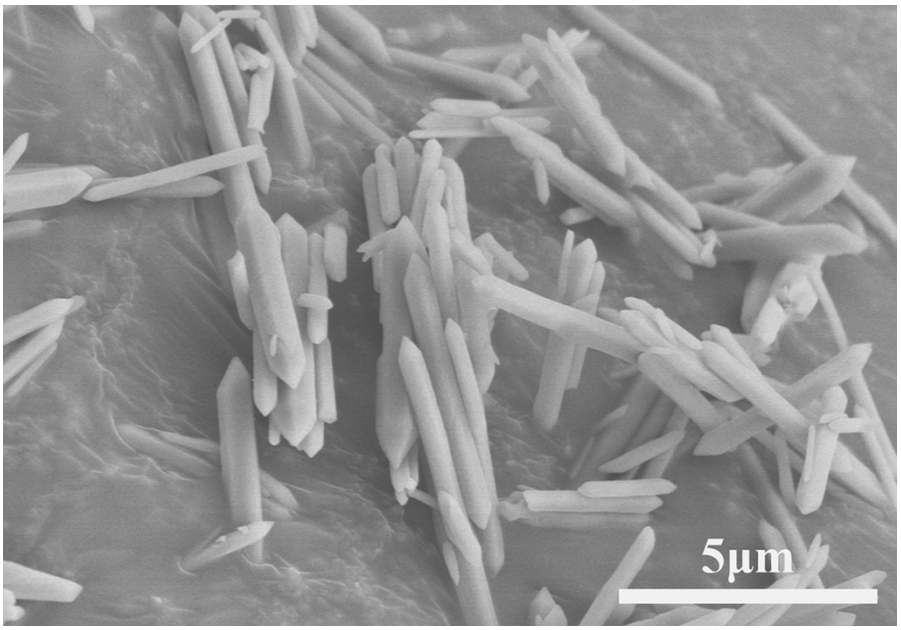

Fig. S4. SEM image of MIL-88A.

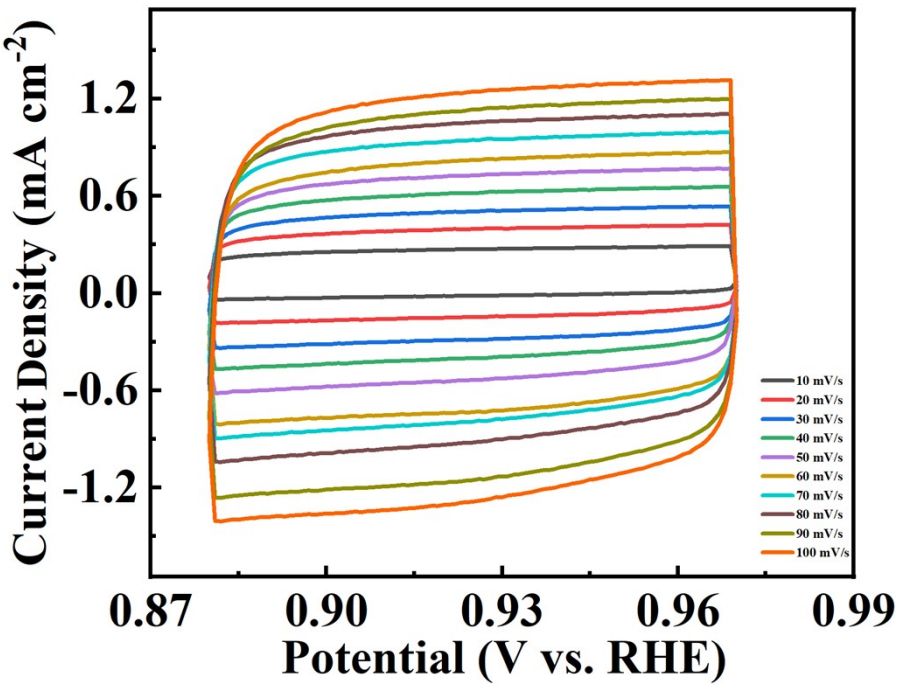

Fig. S5. CV curves of **Ni/Fe-Fe_2O_3@NCNTs** under different scanning rates.

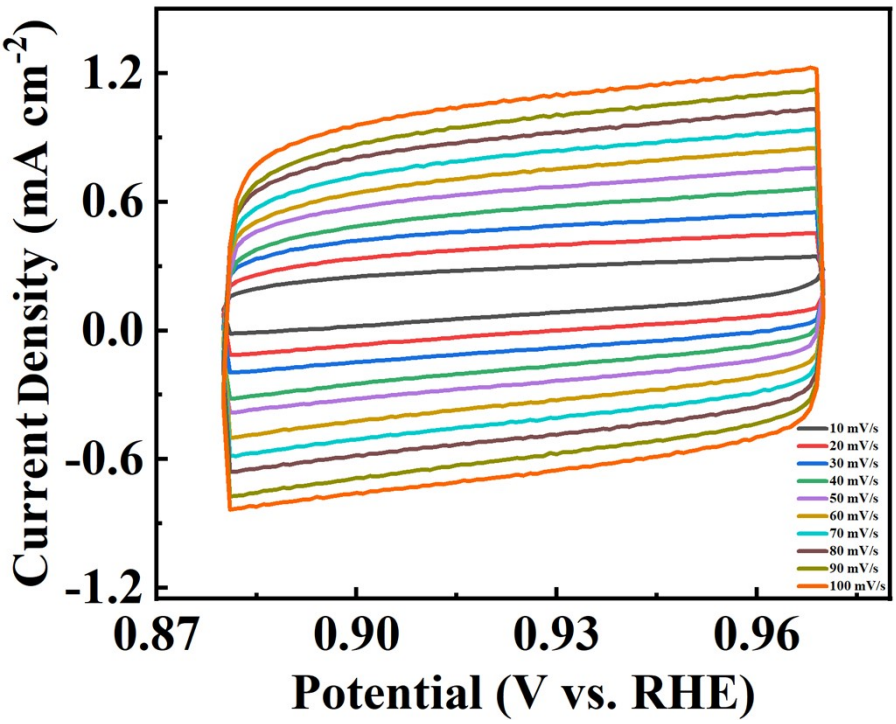

Fig. S6. CV curves of **Fe-Fe_2O_3@NCNTs** under different scanning rates.

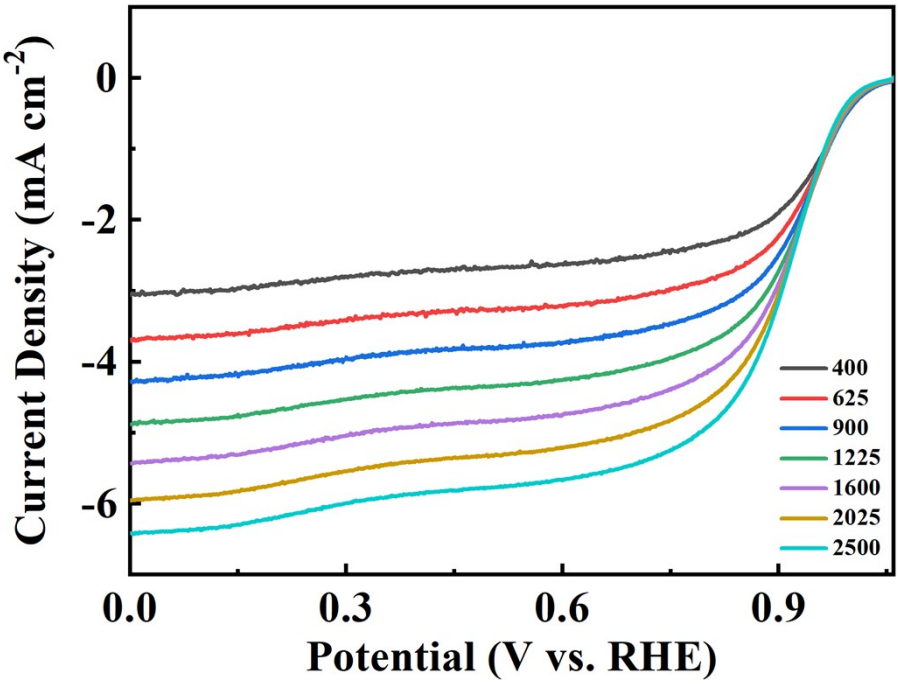

Fig. S7. LSV curves of **Fe-Fe_2O_3@NCNTs** under different rotating rates.

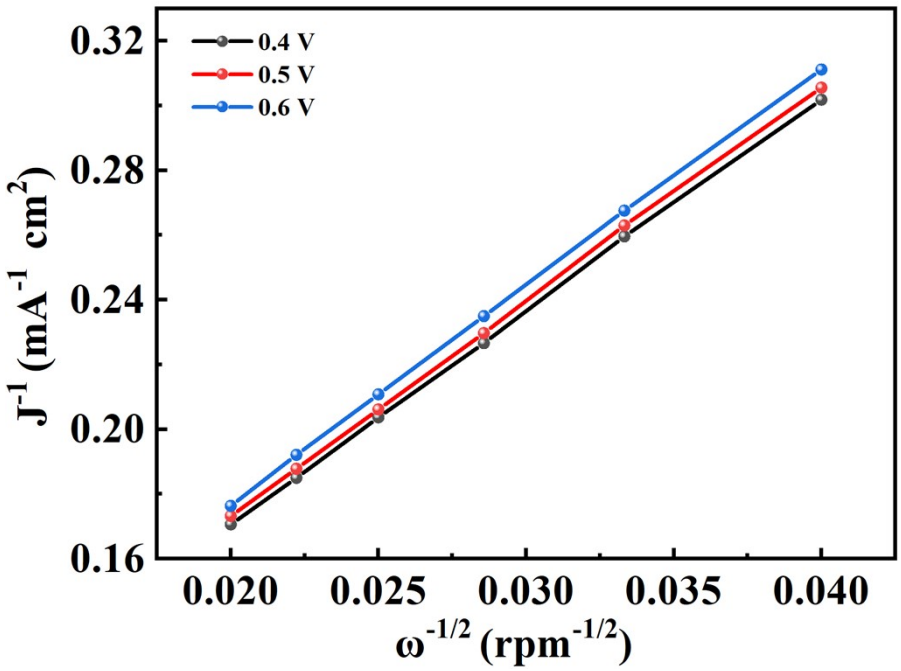

Fig. S8. K-L equation simulation for **Fe-Fe_2O_3@NCNTs**.

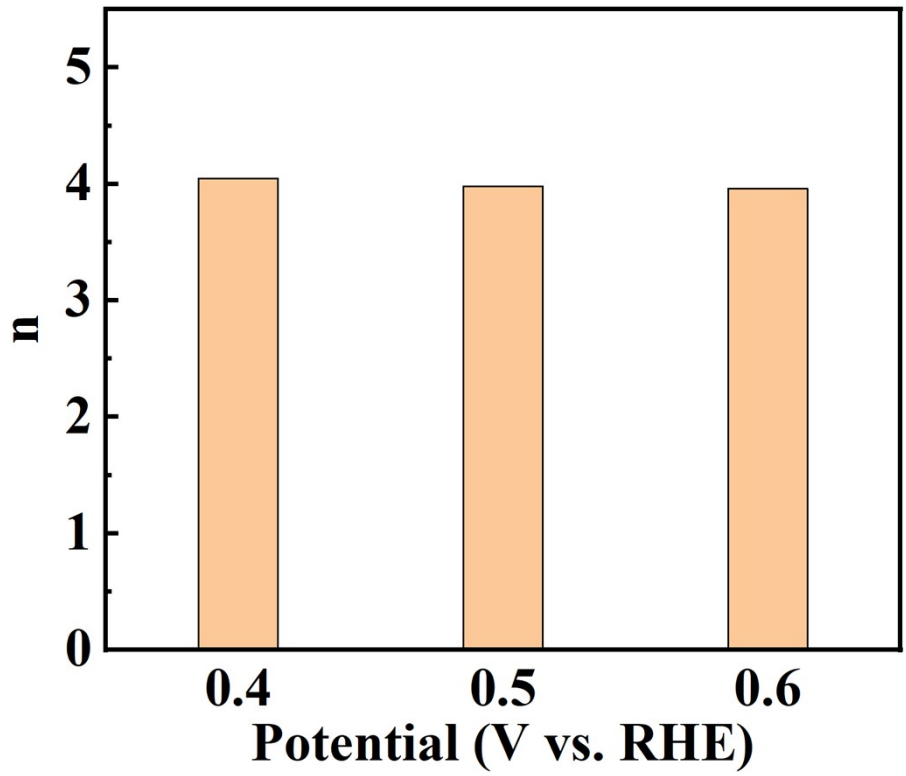

Fig. S9. n values of **Fe-Fe_2O_3@NCNTs** under different potentials.

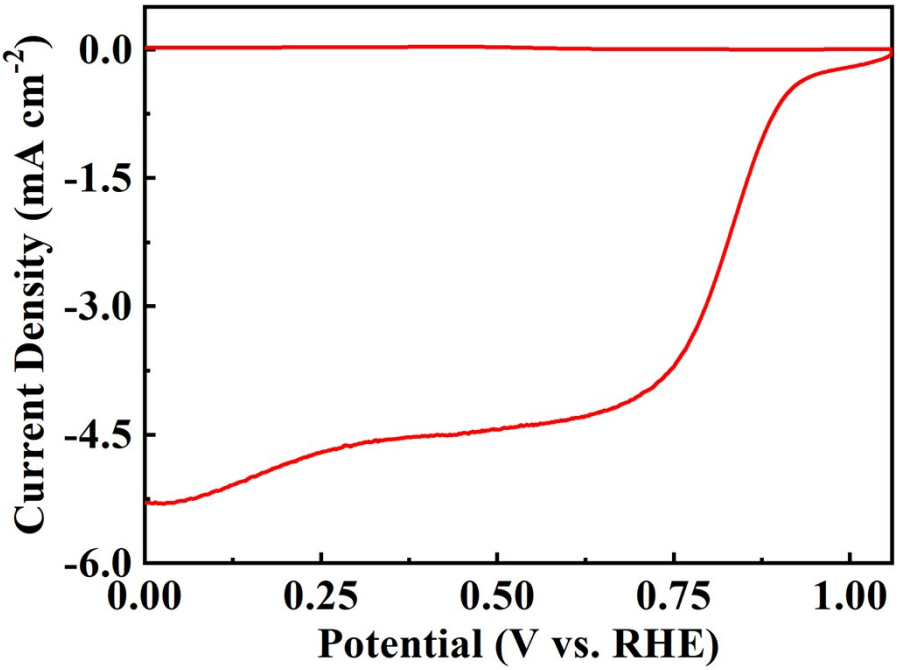

Fig. S10. RRDE voltammograms of **Fe-Fe_2O_3@NCNTs**.

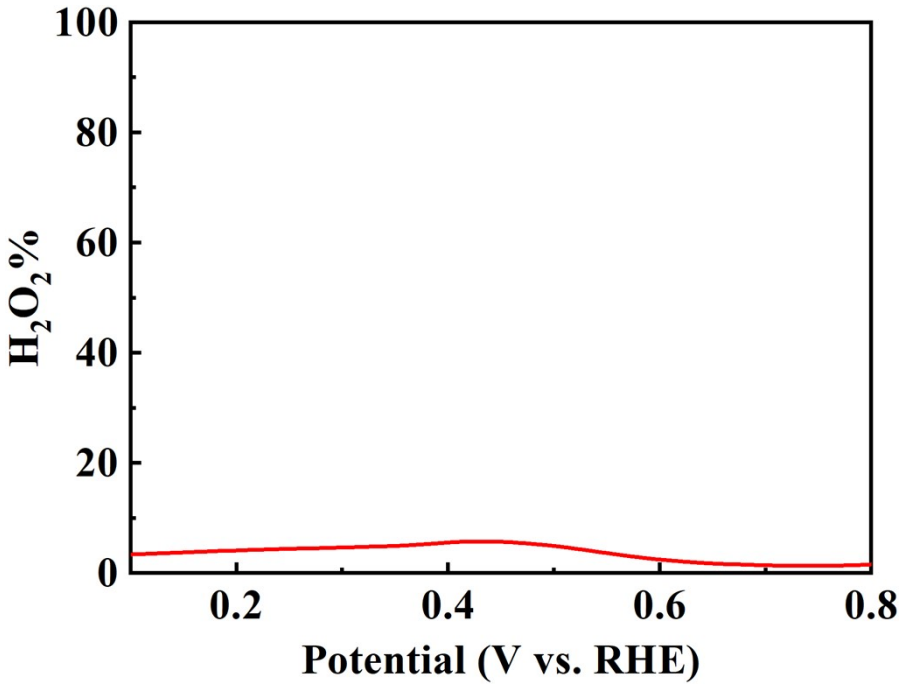

Fig. S11. n value of **Fe-Fe_2O_3@NCNTs**.

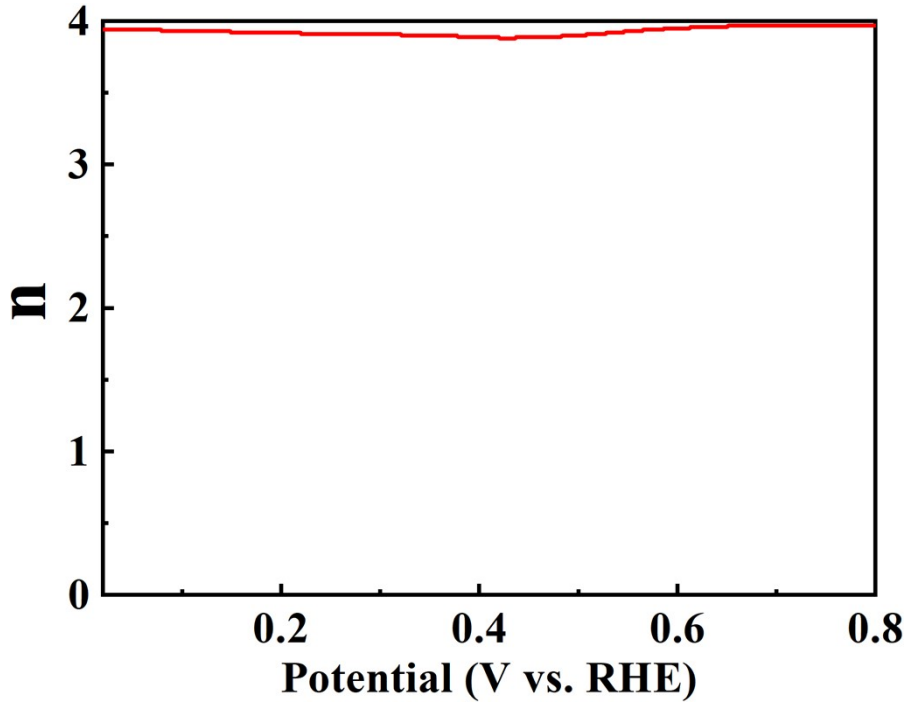

Fig. S12. H_2O_2 selectivity of **Fe-Fe_2O_3@NCNTs**.

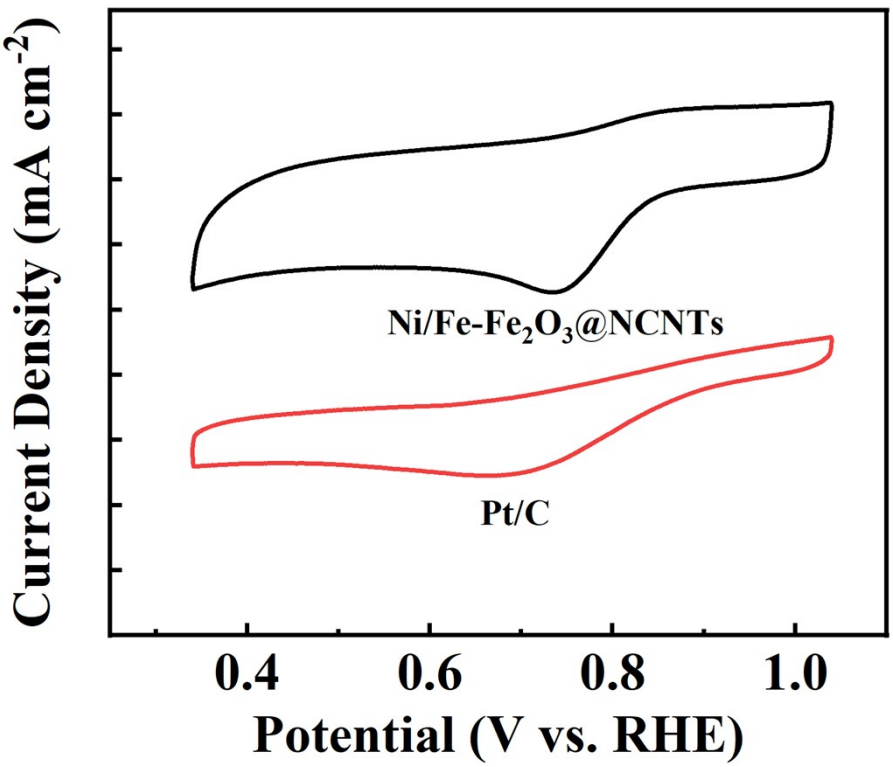

Fig. S13. CV curves of **Ni/Fe-Fe_2O_3@NCNTs** and Pt/C in PBS (0.1 M PBS).

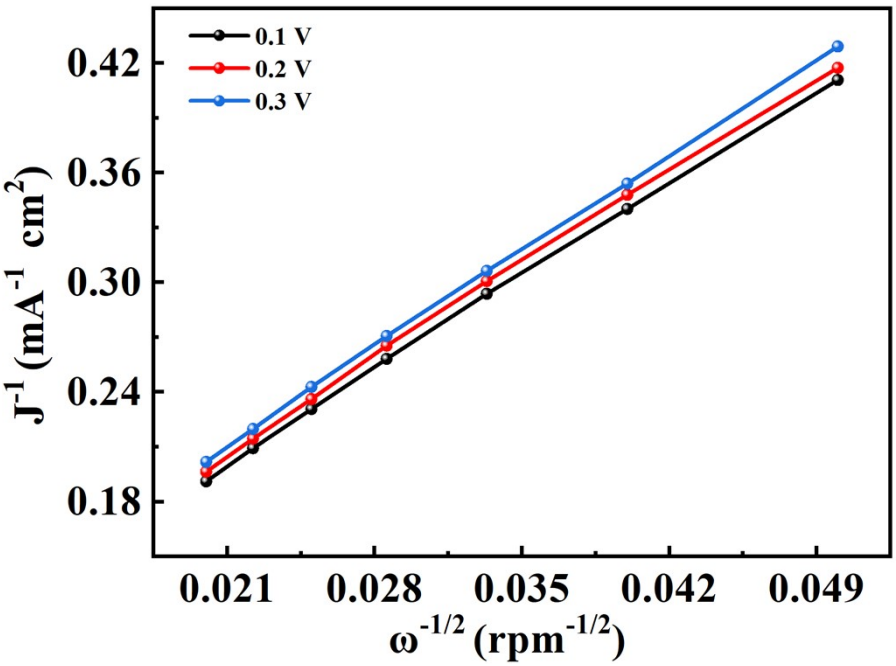

Fig. S14. K-L equation simulation for **Fe-Fe_2O_3@NCNTs** in PBS (0.1 M PBS).

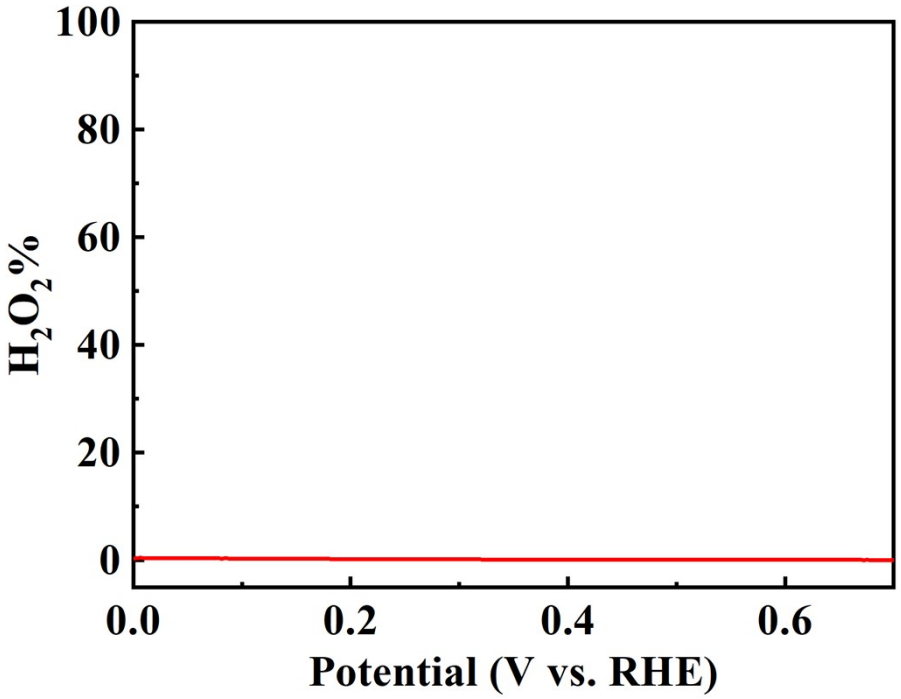

Fig. S15. H_2O_2 selectivity of **Fe-Fe_2O_3@NCNTs** in PBS (0.1 M PBS).

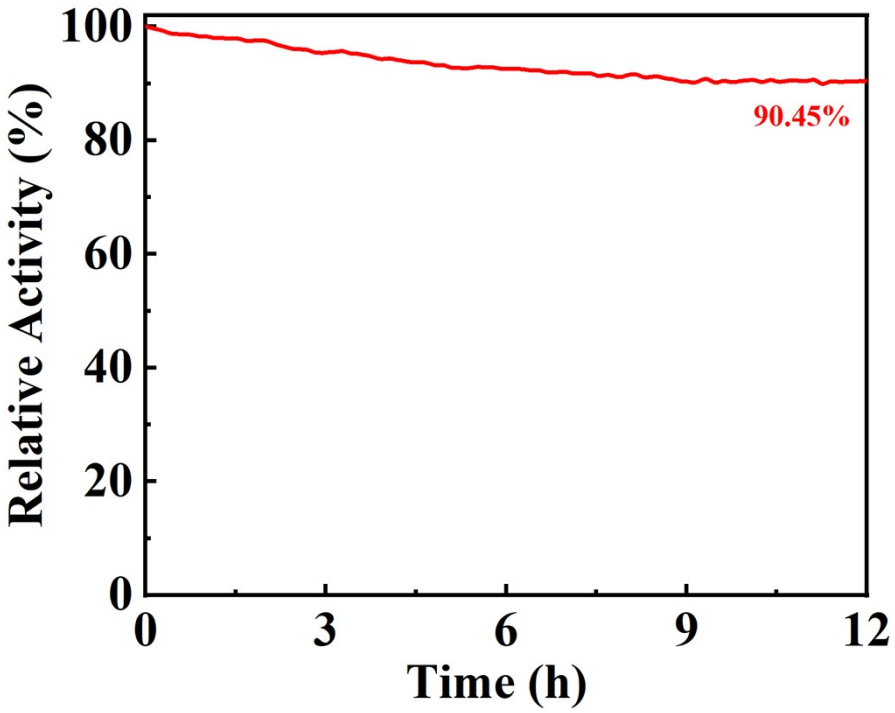

Fig. S16. Chronoamperometric curve of **Ni/Fe-Fe_2O_3@NCNTs** in PBS (0.1 M PBS).

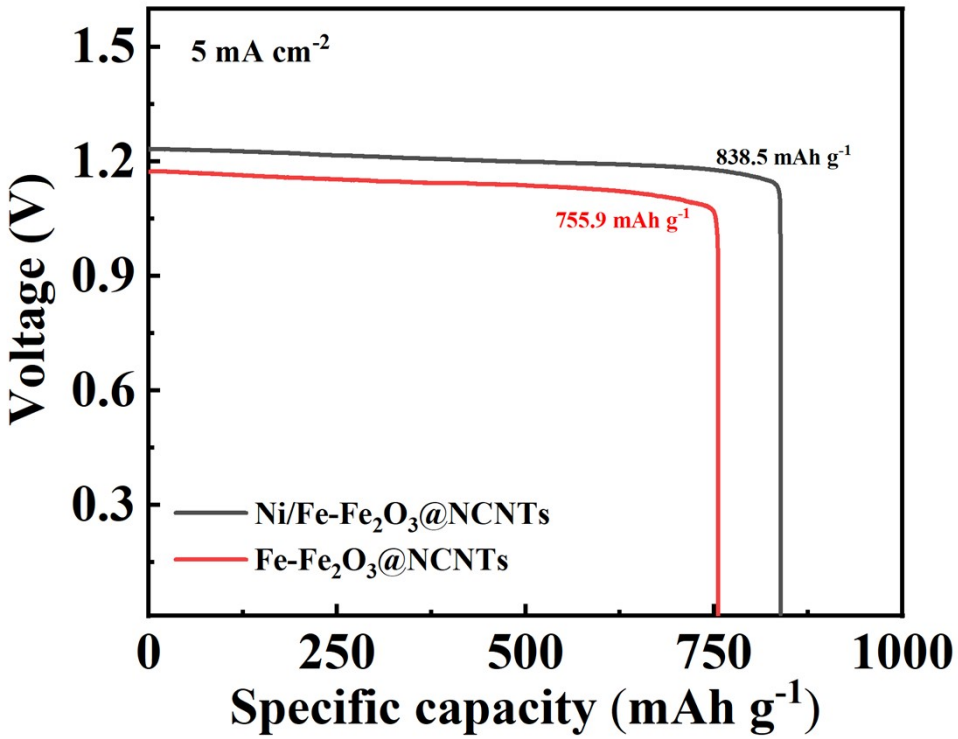

Fig. S17. galvanostatic discharge curves of **Ni/Fe-Fe_2O_3@NCNTs** and **Fe-Fe_2O_3@NCNTs** at 5 mA·cm^{-2}